ACS Catalysis

Research Article

pubs.acs.org/acscatalysis

Support Functionalization To Retard Ostwald Ripening in Copper Methanol Synthesis Catalysts

Roy van den Berg,[†] Tanja E. Parmentier,[†] Christian F. Elkjær,[‡] Cedric J .Gommes,[§] Jens Sehested,[‡] Stig Helveg,[‡] Petra E. de Jongh,[†] and Krijn P. de Jong*,[†]

[†]Inorganic Chemistry and Catalysis, Debye Institute for Nanomaterials Science, Utrecht University, Universiteitsweg 99, 3584 CG Utrecht, Netherlands

[‡]Haldor Topsoe A/S, Nymøllevej 55, DK-2800 Kgs. Lyngby, Denmark

[§]Department of Chemical Engineering, University of Liège B6A, Allée du 6 août 3, B-4000 Liège, Belgium

Supporting Information

ABSTRACT: A main reason for catalyst deactivation in supported catalysts for methanol synthesis is copper particle growth. We have functionalized the support surface in order to suppress the formation and/or transport of mobile copper species and thereby catalyst deactivation. A Stöber silica support was functionalized by treatment with aminopropyltriethoxysilane, which introduces aminopropyl groups on the surface. Copper was deposited on both unfunctionalized and functionalized Stöber silica via incipient wetness impregnation with aqueous copper nitrate solutions followed by drying and calcination. Similar particle size distributions (1−5 nm) were obtained for both supports by changing the flow of N_2 to a flow of 2% NO/N_2 during calcination of the unfunctionalized and amine-functionalized silica, respectively. The effect of support functionalization with aminopropyl groups was an increased stability in the methanol synthesis reaction (40 bar, 260 °C, 23% CO/7% CO_2/60% H_2/10% Ar, 3% CO_x conversion) due to more limited copper particle growth as determined by transmission electron microscopy (TEM). Changing the interparticle distance did not have an influence on the deactivation rate, while the addition of few very large copper particles did, indicating that Ostwald ripening was most probably the dominant particle growth mechanism for these samples. In situ TEM images showed the contact angle between the reduced copper particles and the support. As shape and size was similar on silica as on amine-functionalized silica, the thermodynamic stability of the copper particles was unaltered. The driving force for copper particle growth was thus unchanged upon functionalization. We therefore suggest that Ostwald ripening in methanol synthesis catalysts was retarded by inhibiting the transport of copper species over the support surface. Diffuse reflectance infrared Fourier transform spectroscopy (DRIFTS) revealed a decrease in the number of surface groups (hydroxyl, methoxy, and aminopropyl) upon functionalization because aminopropyltriethoxysilane reacted with multiple hydroxyl groups. Because of that, the distance between neighboring functional groups was increased, suppressing the mobility of Ostwald ripening species from one copper particle to another.

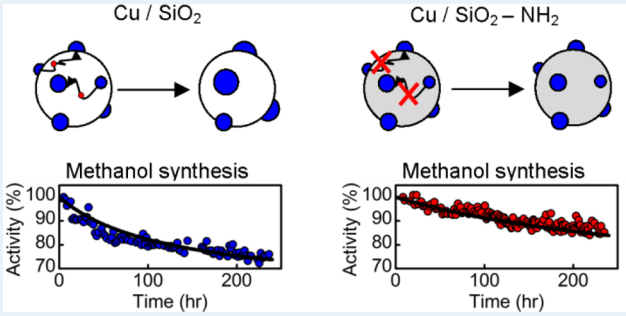

KEYWORDS: *methanol synthesis, copper, support functionalization, Ostwald ripening, deactivation*

INTRODUCTION

Metal particle growth is one of the main causes for catalyst deactivation.[1] Cobalt and iron catalysts in the Fischer−Tropsch reaction,[2] platinum and palladium in the three-way catalyst,[3] nickel catalysts in the methanation reaction,[4] and copper catalysts in the water−gas shift and methanol synthesis reaction[5] all deactivate due to particle growth. The coarsening of particles leads to a decrease in metallic specific surface area and hence activity, and can also change the selectivity for structure-sensitive reactions.[6]

Two main particle growth mechanisms have been postulated in the literature.[7] One mechanism is the migration of entire particles across the support followed by their coalescence.[8] The other mechanism involves the detachment of metal species from one particle followed by transport across the support or in the vapor phase and by subsequent attachment to another particle.[9] The concentration of metal species around a certain particle depends on the thermodynamic stability of the particle in comparison to the stability of the metal species in such a way that smaller particles are less stable and have a higher concentration of metal species in their vicinity, as compared to larger particles. As a result, a concentration gradient of metal species is established between particles with different sizes leading to a net flux of metal species from smaller to larger particles and hence growth of larger

Received: April 22, 2015
Revised: June 11, 2015
Published: June 12, 2015

 © 2015 American Chemical Society

DOI: 10.1021/acscatal.5b00833
ACS Catal. 2015, 5, 4439−4448

particles at the expense of smaller particles—a process often referred to as Ostwald ripening. Irrespective of the mechanism, particle growth is generally considered to depend on catalyst characteristics such as the particle size (distribution),[3b,10] interparticle spacing,[11] support geometry,[12] and metal−support interaction.[12b,13]

Catalysts based upon copper, such as $Cu/ZnO/Al_2O_3$, are used in industry in the water−gas shift and the methanol synthesis reaction. The worldwide production of methanol is about 65 million metric tons a year. The produced methanol is used as a building block for other products like methyl *tert*-butyl ether (MTBE), acetic acid, and formaldehyde.[14] Furthermore, methanol can be converted into olefins via the methanol to olefins (MTO) process or can be used in the future to store renewable energy.[15] In the $Cu/ZnO/Al_2O_3$ catalyst, copper acts as the catalytically active metal, zinc oxide as a chemical promoter, and alumina as a structural promoter.[14,16] Typically, one-third of the initial activity of the catalyst is lost during the first 1000 h of operation, with copper particle growth being the main reason for deactivation.[5,14] The reaction temperature (480−580 K) is well below the Tammann temperature of copper (680 K), indicating that thermal migration of atoms in the absence of a reactive adsorbate is unlikely.[14] This is further illustrated by the strong dependence of the deactivation on the composition of the synthesis gas.[17] Copper particle growth in the methanol synthesis reaction is therefore probably mediated by mobile copper species either on the copper surface (effectively changing the center of mass resulting in particle migration) or on the support surface (resulting in Ostwald ripening).[5,11a,18] Suppressing the formation and/or transport of these mobile species is therefore of paramount importance to retard deactivation. In the case of Ostwald ripening, the rate of formation of these species depends on the thermodynamic stability of the metallic particles and of the metal species, which both depend on the chemical nature of the support surface.[19] Moreover, the transport of mobile metal species over a support also depends upon the chemical nature of the support surface. In this contribution, we report on our efforts to determine the effect of functionalizing the surface of a support on particle growth during the methanol synthesis reaction.

Support functionalization was performed by introducing aminopropyl groups onto the surface of Stöber silica.[20] The synthesized Stöber silica consisted of nonporous spheres of around 40 nm in diameter, enabling the functionalization of its surface without significantly changing its porosity or geometry.[21] Functionalization was carried out before copper deposition to avoid blocking the active metal sites (see Supporting Information). Incipient wetness impregnation with aqueous copper nitrate solutions was performed to deposit copper on the (un)functionalized silica support. Heat treatment was performed in either N_2 or in 2% NO/N_2, resulting in different decomposition pathways of the copper nitrate.[22] The performance of the synthesized catalysts in the methanol synthesis reaction was determined at 40 bar of 7% CO_2, 23% CO, 60% H_2 and 10% Ar at 260 °C for 10 days. The catalysts were retrieved after the reaction to determine the extent of copper particle growth.

■ EXPERIMENTAL SECTION

Stöber Silica Support. Nonporous silica spheres of 30−50 nm in diameter were synthesized via a procedure adapted from Stöber et al.[21b] Initially, 230 mL of ethanol and 11.25 mL of ammonia (NH_3, Merck, 25% solution for analysis) in a PET bottle were heated to 35 °C and stirred at 230 rpm. Subsequently, 17.3 g of tetraethyl orthosilicate (TEOS, Aldrich, 98%) was instantaneously added. The solution was left for 15 h at 35 °C at 230 rpm to ensure full conversion of TEOS into silica. After this time, the solution was neutralized with 8.5−9 mL of nitric acid (HNO_3, Merck, 65% for analysis), and the liquid was removed using a rotary evaporator. The silica was then dried overnight at 120 °C and calcined in air according to the following three-step schedule: 2 h at 200 °C (100 °C/h) to remove all remaining water, 1 h at 400 °C (100 °C/h) to decompose unreacted ethoxy silicates, and 3 h at 600 °C (100 °C/h) to decrease the microporosity within the silica spheres. The yield of the synthesis was 4.8 g silica (96 wt %).

Functionalization. Functionalization of the Stöber silica with aminopropyl groups was performed according to a procedure from Jacinto et al.[20e] and Oliveira et al.[20d] Aminopropyl groups were introduced on the silica surface via a reaction between aminopropyltriethoxysilane (APTES, Aldrich, 99%) and hydroxyl groups. To avoid self-hydrolysis of APTES due to the presence of water, the functionalization was carried out under inert N_2 atmosphere using standard Schlenk techniques and dry organic solvents. First, 0.8 g silica was dried overnight at 120 °C under vacuum. Then, 50 mL of 1 vol % APTES in toluene (Interchemica, > 99.99%, dried with an mBraun MB SPS-800 column) was added dropwise under vigorous stirring. The suspension was stirred for 2 h at room temperature. After that, the mixture was centrifuged for 5 min at 5000 rpm. The solvent was decanted and the silica was washed twice with dry toluene and once with ethanol (Interchemica, 100%) using centrifugation. The obtained functionalized silica was dried overnight at 60 °C in air.

Copper Deposition. Copper was deposited via incipient wetness impregnation followed by drying and calcination. Before impregnation, the supports were dried at 150 °C under vacuum for 1 h to remove adsorbed water. After that, the supports were impregnated with 0.25 to 1 M of aqueous copper nitrate ($Cu(NO_3)_2{\cdot}3H_2O$, Acros Organics) in 0.1 M HNO_3, followed by drying overnight under vacuum at room temperature. Subsequently, the samples (∼2 g) were heated at 350 °C (2 °C/min) in a plug flow reactor with either 750 mL/min N_2 or 375 mL/min of 2% NO/N_2.[22] Table 1 shows a list of the prepared samples.

Catalytic Testing. The performance of the catalysts in the methanol synthesis reaction was investigated in a continuous fixed-bed stainless steel reactor with an inner diameter of 0.9 cm (Autoclave Engineers). The calcined catalysts were pressed, crushed, and sieved to obtain a sieve fraction of 425 to 630 μm. 0.6−0.9 g (bed height of 3−5 cm) of the catalysts was loaded into the reactor and reduced in situ at 250 °C (2 °C/min) for 2.5 h with a flow of 110 mL/min 20% H_2/Ar. After that, the temperature was lowered to 100 °C to prevent premature production of methanol when switching to syngas. The reactor was flushed with syngas (10% Ar, 7% CO_2, 23% CO, 60% H_2, Linde), which was purified with a metal carbonyl trap[24] (4.0 g of H-USY zeolite, CVB-780 from Zeolyst Int., 0.5−1.5 mm and 5 g of activated carbon, Norit R3B). The argon was added to the syngas feed as an internal standard for the gas chromatograph (GC). After 30 min of flushing, the pressure was increased to 40 bar. From this time on, the exit gas composition was measured every 110 min with a GC (Varian 450). The lines from the reactor to the GC were heated to 150 °C to avoid any methanol or water condensation. The first GC channel consisted of a HAYESEP Q (0.5 m × 1/8 in.) column followed by a MOLSIEVE 13x (15 m × 1/8 in.) column that led to a thermal conductivity detector (TCD). The second GC channel consisted

DOI: 10.1021/acscatal.5b00833
ACS Catal. 2015, 5, 4439−4448

Table 1. Sample List

sample name	density surface groups (nm^{-2})	$[Cu^{2+}]$ (M)	Cu (wt %)	surface density copper atoms (nm^{-2})	molar ratio OH or NH_2 to Cu	heat treatment
S	4.6 OH	-	-	-	-	-
CS_1a	4.6 OH	0.25	0.9	0.9	5	N_2
CS_1b	4.6 OH	0.25	0.9	0.9	5	NO/N_2
CS_2a	4.6 OH	0.50	1.8	1.8	2.5	N_2
CS_4a	4.6 OH	1	3.5	3.5	1.3	N_2
SN	2.6 NH_2	-	-	-	-	-
CSN_1a	2.6 NH_2	0.25	0.8	1.2	2.2	N_2
CSN_1b	2.6 NH_2	0.25	0.8	1.2	2.2	NO/N_2

The sample designations are as follows: S stands for Stöber silica, C for copper and N for NH_2 surface groups. 1, 2, and 4 refer to the copper concentration used during incipient wetness impregnation: 1 is 0.25 M, 2 is 0.5 M, and 4 is 1 M of copper nitrate. a or b correspond to the heat treatment used after impregnation and drying: a is heat treatment in N_2 at 350 °C. b is heat treatment in 2% NO/N_2 at 350 °C. The nominal amount of copper atoms per nm^2 support is calculated using the experimental BET surface areas of the supports. The nominal amount of OH groups per nm^2 support is based upon work from Zhuravlev et al.[23] The nominal amount of NH_2 groups per nm^2 support is based upon the amount of aminopropyl groups introduced on Stober silica (~1.8 wt %, ICP and TGA) and the BET surface area of SN.

of a CP-L 8CB FS capillary column that led to a flame ionization detector (FID). After reaching 40 bar, the temperature was increased to 260 °C (2 °C/min) to produce methanol. The amount of catalyst and the syngas flow (10−30 mL/min) were chosen such that CO_x conversion levels near 3% were obtained. The activity of the catalysts was calculated from the conversion of CO plus CO_2 during reaction (see Supporting Information). Turn over frequencies (TOF) were calculated with the assumption that each copper surface atom was an active site. The copper dispersion was based upon TEM particle size distributions assuming spherical particles and calculated with the formula: dispersion = $6V_m/(A_m \times PS) = 1.04/PS$, where V_m is the molar volume, A_m the molar area, and PS the surface averaged particle size in nanometer. For CS_4a, the copper dispersion was calculated assuming that 2.1 wt % (EDX) of the copper was present in 2−3 nm particles and that the remaining 1.4 wt % was present in particles larger than 100 nm, resulting in an negligible contribution of these large particles to the total copper surface area. The selectivity was determined from the FID chromatograms and was in all cases more than 95% toward methanol, with dimethyl ether as the main side product. The stability of the methanol productivity over time was based upon the methanol signal from the TCD detector. Second-order deactivation curves were fitted according to the formula: $(a - a_s)^{-1} = k_{d,2} \times t + 1/(1 - a_s)$,[1] in which a is the activity. "a_s" is the normalized activity at $t = \infty$ (for all catalysts 60% of the initial activity), $k_{d,2}$ is the second-order deactivation constant, and t is the time.

Characterization. N_2-physisorption measurements were done with a Micromeritics Tristar 3000 V6.08 at liquid nitrogen temperature. Prior to the measurements, the samples were outgassed at 130 °C in a nitrogen flow for 14h. The Brunauer−Emmett−Teller (BET) method was used to determine the specific surface area.[25] The pore volume was determined at $p/p_0 = 0.9975$. BJH method analysis of the desorption branch was used to obtain the average pore size. The t-plot method was used to determine the micropore volume. X-ray diffraction was performed with a Bruker-Nonius D8 Advance X-ray diffractiometer using Co $K\alpha_{12}$ (λ = 1.79026 Å) radiation. Diffractograms were obtained at room temperature from 20° to 70° (2θ). Diffuse reflectance infrared Fourier transform spectroscopy (DRIFTS) spectra were recorded with a Bruker Tensor 27 using a HVC-DRP-3 diffuse reflectance reaction chamber with CaF_2 windows and a mercury−cadmium−telluride (MCT) detector. The sample cup holder was filled for 2/3 with silicon carbide, covered by a grid on which ~15 mg of sample was placed. The sample was dried in situ prior to the measurement at 200 °C (2 °C/min) with a N_2 flow of 10 mL/min. Spectra were recorded after cooling to room temperature and normalized to the SiO_2 peak at 1860 cm^{-1}.[26] The chemical composition of the catalysts was determined with inductively coupled plasma (ICP) analysis at the Mikroanalytisches Laboratorium Kolbe (Mülheim an der Ruhr, Germany) using optical emission spectra (OES), recorded with a PerkinElmer spectrometer. Thermogravimetric analysis (TGA) of the samples was measured with a PerkinElmer Pyris 1 TGA device. After drying for 20 min at 30 °C, 10 mg of sample was heated to 600 °C (5 °C/min) in a flow of 10 mL/min O_2. Temperature-programmed reduction (TPR) measurements were done with a Micromeritic Autochem II ASAP 2920. Prior to the measurements, the samples were dried at 120 °C for 30 min. After cooling, the temperature was increased to 800 °C (5 °C/min) under a flow of 5% H_2/Ar. During this treatment, the H_2 concentration was determined with a thermal conductivity detector (TCD).

Transmission Electron Microscopy. Samples for transmission electron microscopy (TEM) were prepared by crushing them followed by sonication in ethanol. A droplet of this suspension was deposited onto a carbon coated copper TEM grid (Agar S162 200 Mesh Cu, Van Loenen instruments). TEM images were acquired with a Tecnai 12 (FEI) electron microscope operated with a primary electron energy of 120 kV. For each sample, at least 200 particles were analyzed with respect to their size by measuring the apparent diameter (see Supporting Information for the relation between the apparent diameter and the radius of curvature). Before reaction, the images were taken of the samples after calcination. After reaction, the samples were passivated for 15 min by exposing the samples at room temperature to a diluted air/argon flow by creating a small leak in the flow supply system. Before taking TEM images, the samples were furthermore exposed for a limited time (<2 h) to air. In general, this treatment results into a (partial) oxidation of the copper particles as evidenced by the appearance of CuO and/or Cu_2O peaks in XRD and CuO and/or Cu_2O lattice fringes in high-resolution TEM. Taking into account the densities of Cu and CuO, the increase in particle size upon full oxidation is around 15%. The Kirkendall effect, which results in hollow particles after oxidation, was never observed for particles smaller than 8 nm. The effect of the oxidation state on the particle size distribution was therefore minor and within the statistical error of the measurements. Energy dispersive X-ray (EDX) spectroscopy was performed on a Tecnai 20FEG (FEI) electron microscope equipped with a field emission gun with an EDAX Super Ultrathin Window (SUTW) EDS detector and processed with Tecnai Imaging and Analysis software (TIA). For this, CS_4a was placed on a carbon coated Ni TEM grid (Agar 162 200 Mesh Ni, Van Loenen instruments). Several regions (1 × 1 μm) without very large (>100 nm) particles were analyzed.

In situ TEM was performed using an image aberration corrected Titan 80−300 SuperTwin ETEM (FEI Company) operated at a primary electron energy of 300 keV. Prior to the

DOI: 10.1021/acscatal.5b00833
ACS Catal. 2015, 5, 4439−4448

experiment, the image aberration corrector was tuned using an Au/C cross-grating (Agar S106), and the spherical aberration coefficient was set in the range of −10 to −20 μm. TEM samples of CSN_1a, CSN_1b and CS_1a were prepared by grinding and dispersing the resulting powder on stainless steel grids. The samples were inserted in the microscope using a Gatan heating holder (model 628). CSN_1a was reduced at 250 °C at 1 mbar H_2 for 0.5 h and TEM images were subsequently acquired under similar conditions with a bottom-mounted 2k × 2k charged-coupled device (Gatan US1000). Initial images were taken at a low dose rate of 20 $e^-/Å^2s$. Subsequently, the electron dose was increased to 100 $e^-/Å^2s$ and images were acquired after 20 min exposure. CSN_1b and CS_1a were reduced at 300 °C at 1 mbar H_2 for 0.5 h and TEM images were subsequently acquired at these conditions. To assess the effect of the electron beam on the apparent contact angle of the copper particles, first an overview image was taken at a low dose rate of 5 $e^-/Å^2s$. Subsequently, the dose rate was increased to 100 $e^-/Å^2s$ to obtain higher magnification images. Lastly, the electron dose was decreased to 5 $e^-/Å^2s$ to assess the changes in the sample upon exposure to 100 $e^-/Å^2s$. An effect of the electron exposure upon the apparent contact angle was not observed.

RESULTS

Supports. TEM showed that the synthesized Stöber silica (S) consisted of 30−50 nm silica primary spheres (Figure 1). These spheres were partly fused together forming larger aggregates as shown by electron tomography (see Supporting Information). The TEM images further showed a uniform contrast across the Stöber spheres, suggesting the absence of micropores, which agrees with N_2-physisorption results (Table 2, caption).

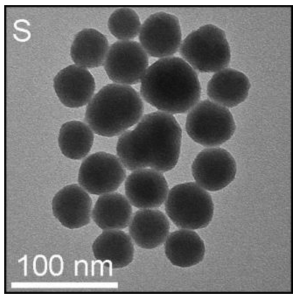

Figure 1. TEM image of Stöber silica (S).

Table 2. N2 Physisorption

sample	SA (m^2/g)	PV (cm^3/g)	pore size (nm)
S	100	0.58	20
SN	75	0.53	26

N_2-physisorption data of Stöber silica (S) and Stöber silica functionalized with NH_2 groups (SN). The BET surface area (SA), pore volume (PV) and average pore size of the supports are given in the table. For both materials the micropore volume was <0.01 cm^3/g.

Upon functionalization, the three ethoxy groups of aminopropyltriethoxysilane (APTES) can react with a maximum of three hydroxyl groups at the surface of the silica (Figure 2A). Assuming 4.6 OH groups per nm^2 of silica surface[23] and taking into account the specific surface area of the Stöber silica, the theoretical amount of introduced functional groups is 1.4 wt % (0.9 wt % carbon, 0.3 wt % nitrogen and 0.2 wt % hydrogen).

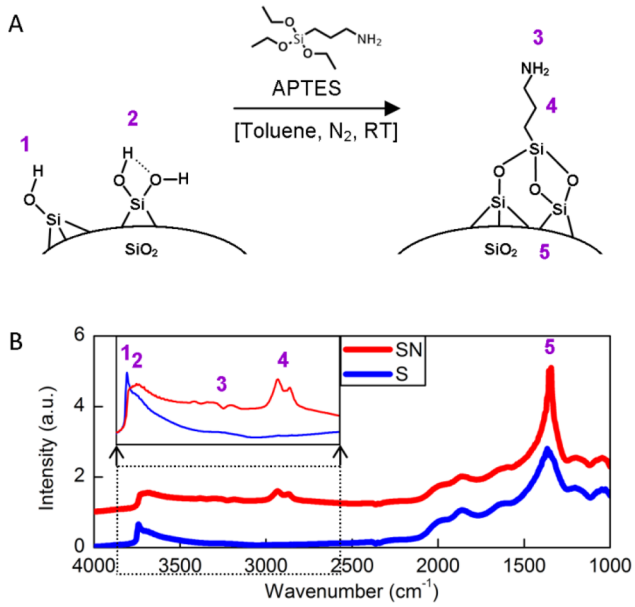

Figure 2. (A) Schematic representation of one possible reaction between hydroxyl groups and APTES. (B) DRIFTS spectra of Stöber silica (S) and amine-functionalized Stöber silica (SN). The different peaks are numbered and correspond to the groups numbered in (A). The inset on the top left of the image is a blow-up of the spectrum from 3800 to 2600 cm^{-1}. No vertical offset is used herein.

Elemental analysis with inductively coupled plasma (ICP) showed a carbon content of 1.36 wt % and a nitrogen content of 0.36 wt % after functionalization (SN). Thermal gravimetric analysis (TGA) in an oxygen flow up to 600 °C showed a weight loss of 1.8 wt % for sample SN, whereas no weight loss was observed for the parent Stöber silica sample (S). The weight loss for sample SN was thus ascribed to the decomposition of aminopropyl groups. Both techniques suggested a slightly higher amount of aminopropyl groups in the sample than theoretically expected. The small excess might be due to self-hydrolysis of one or more of the APTES ethoxy groups, effectively lowering the number of hydroxyl groups that bind APTES. After functionalization of the Stöber silica, both the specific surface area and pore volume had decreased due to the addition of aminopropyl groups (Table 2).

Figure 2B shows DRIFTS spectra of Stöber silica before and after functionalization. The peaks below 2200 cm^{-1} are assigned to the stretching modes of Si−O−Si and dangling modes of Si−O.[26] This part of the spectrum is similar for both supports because they both consisted mainly of silica. On the functionalized support, peaks originating from C−H and N−H vibrations appeared. The peaks at 2875 and 2940 cm^{-1} are assigned to C−H vibrations originating from the propyl chain of the functional groups.[27] The peak at 3320 cm^{-1} is attributed to the asymmetric N−H stretch vibration, and the peak at 3380 cm^{-1} is assigned to the symmetric N−H stretch vibration in aminopropyl groups.[27,28] The broad peak of the O−H stretch vibration at 3615 cm^{-1}, ascribed to hydrogen bonded hydroxyl groups, remained present after functionalization.[28] The O−H stretch vibration at 3745 cm^{-1} is attributed to isolated hydroxyl groups and was largely reduced upon functionalization due to the reaction with APTES.[28] The functionality of the surface was thus successfully altered by the addition of aminopropyl groups at the expense of isolated hydroxyl groups.

DOI: 10.1021/acscatal.5b00833
ACS Catal. 2015, 5, 4439−4448

Copper. Six different catalysts were made via incipient wetness impregnation of the (functionalized) silica supports with aqueous copper nitrate followed by drying and heat treatment in N_2 or 2% NO/N_2 (Table 1). The first set was prepared by impregnating nonfunctionalized Stöber silica with 0.25 M, 0.5 and 1 M of copper nitrate followed by calcination in N_2 flow. Representative TEM images of the samples after calcination are shown in Figure 3A–D. The resolution of the microscope and the structure of the catalysts allowed us to detect copper oxide particles down to ca. 1.5 nm.

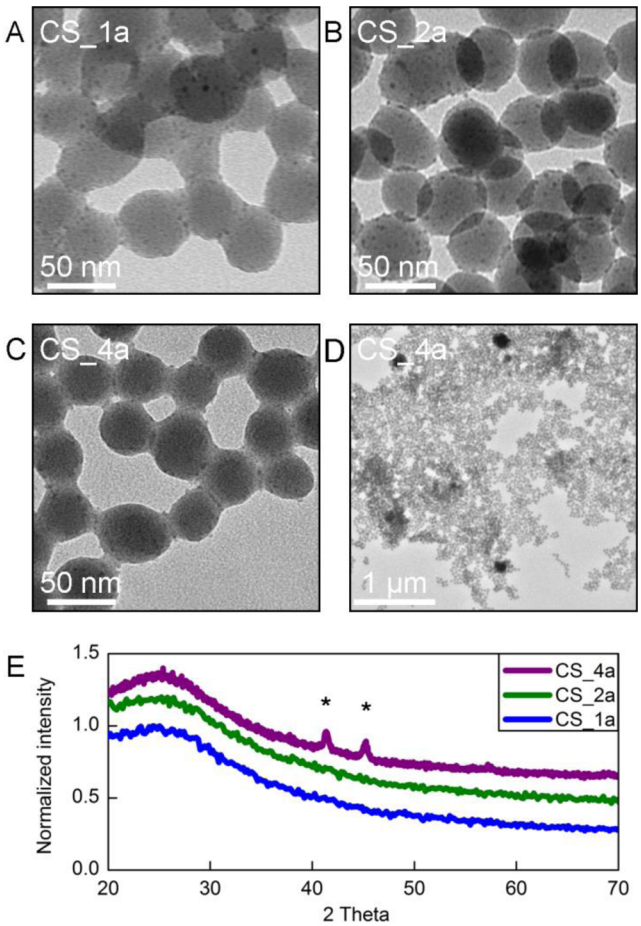

Figure 3. TEM images of (A) CS_1a, (B) CS_2a and (C, D) CS_4a. (E) X-ray diffractograms of the samples; designated peaks (*) correspond to CuO. All samples contain 2–3 nm sized copper oxide particles, as visualized with TEM. For CS_4a, however, the presence of large (>100 nm) particles was also detected with TEM. For this sample, XRD confirmed the presence of CuO crystallites larger than 20 nm.

In the case of CS_1a and CS_2a, heat treatment in a flow of N_2 resulted in 2–3 nm sized copper oxide particles (darker image features) homogeneously distributed over the support, in agreement with earlier observations.[11a,29] TEM images of CS_4a revealed additionally to the 2–3 nm sized particles some large (>100 nm) particles (Figure 3C, D). XRD confirmed the presence of large CuO crystallites for this sample (Figure 3E). Energy dispersive X-ray spectroscopy in regions with only 2–3 nm particles showed a local copper loading of around 2.1 ± 0.5 wt %. Because the total copper loading was 3.5 wt %, the remaining 1.4 wt % was present in the large (>100 nm) particles. According to Munnik et al., anhydrous copper nitrate is formed during N_2 calcination.[22] This species is volatile and very mobile and gives rise to copper redispersion over the silica surface. Assuming two surface hydroxyl groups as anchoring site for one molecule copper nitrate and 4.6 OH groups per nm^2 silica,[23] the maximum amount of anchored anhydrous copper nitrate amounts to 2.3 copper complexes per nm^2,[29] which corresponds to a copper loading of 2.3 wt % for Stöber silica. For CS_1a and CS_2a, the copper loading was lower, so all anhydrous copper nitrate was able to anchor to the support. Upon decomposition of the copper nitrate, 2–3 nm copper oxide particles were formed as a result. The copper loading for CS_4a was, however, higher than 2.3 wt % resulting in the aggregation of excess copper nitrate and hence the formation of very large copper oxide particles.

In contrast to copper on silica (CS_1a), TEM images of 0.8 wt % of copper on amine-functionalized silica (CSN_1a) did not show the presence of 2–3 nm particles, not even after in situ TEM reduction at 250 °C at 1 mbar H_2 for 0.5 h (Figure 4A). In

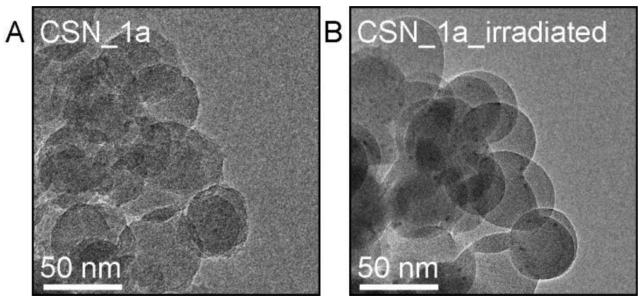

Figure 4. (A) TEM image of CSN_1a at 250 °C at 1 mbar of H_2. No copper particles were detected. (B) The same area as (A) after intense prolonged electron beam exposure (~20 min at 100 $e^-/Å^2$ s). 1–2 nm particles were detected.

fact, no particles were detected at all at low electron dose rates (20 $e^-/Å^2$ s). The usage of a higher electron dose rate (100 $e^-/Å^2$ s) yields a better image signal-to-noise ratio. The higher dose rate in conjunction with longer exposure times (~20 min) resulted in a smoother silica surface and the appearance of 1–2 nm wide particles which are presumably of copper (Figure 4B). Initially, the copper is distributed as atomic species or as particles smaller than 1–2 nm, representing the critical size for unambiguous distinction of features on the silica support. Adsorption of copper nitrate during synthesis was in this case probably via aminopropyl groups. The ratio of aminopropyl groups to copper was for this sample higher than 2 (see Table 1). Increasing the copper loading further might lead to an oversaturation of these groups with copper nitrate, which might result in larger particles similarly to copper on unfunctionalized silica. Sintering of copper species during drying and calcination at the current loading was very limited as evidenced by the absence of particles larger than 1–2 nm after calcination. This indicates that anhydrous copper nitrate, similar to copper ions,[30] was more strongly adsorbed by the aminopropyl groups than by hydroxyl groups, limiting its mobility.

Representative TEM images and particle size distributions of copper on functionalized and nonfunctionalized silica after 2% NO/N_2 calcination (CS_1b and CSN_1b) are shown in Figure 5A–D. For both supports, the size of the copper oxide particles was larger after 2% NO/N_2 calcination than after N_2 calcination (Figure 5A and C vs Figure 3A and 4A, respectively). For copper on nonfunctionalized silica (CS_1b), the heat treatment in 2% NO resulted in particles with sizes ranging from 4 to 15 nm, whereas for copper on functionalized silica (CSN_1b), this

DOI: 10.1021/acscatal.5b00833
ACS Catal. 2015, 5, 4439–4448

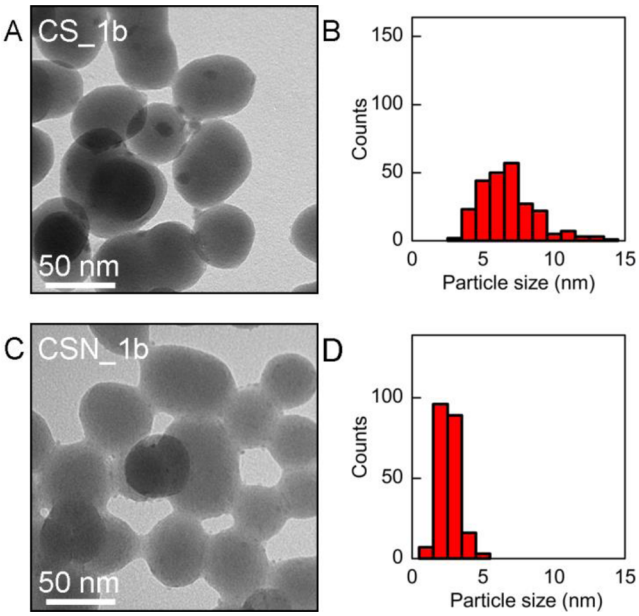

Figure 5. (A) TEM image of CS_1b. (B) Copper oxide particle size distribution of CS_1b determined with TEM. (C) TEM image of CSN_1b. (D) Copper oxide particle size distribution of CSN_1b determined with TEM.

resulted in 2−3 nm particles. The distribution of the particles in CSN_1b seemed to be homogeneous across the support surface. The difference with the N_2 heat treated samples was due to a different decomposition route of copper nitrate to copper oxide in the case of heat treatment in NO. According to Munnik et al., a nonvolatile and nonmobile copper species, $Cu_2NO_3(OH)_3$, is formed upon heating to 110 °C in NO.[22] During the formation of this phase it can grow from mobile copper nitrate, $Cu(NO_3)_2*3H_2O$. The smaller particles for CSN_1b compared to CS_1b indicate that different mobility of such species could explain the observations and that mobility is higher on silica than on amine-functionalized silica. This suggests that aminopropyl groups adsorb not only copper ions and anhydrous copper nitrate but also copper nitrate trihydrate stronger than hydroxyl groups do.

The temperature required to reduce the copper precursors of the heat treated samples to metallic copper was determined with temperature-programmed reduction (TPR). Figure 6 shows the H_2 consumption as a function of temperature up to 350 °C. Above 350 °C, no further hydrogen consumption was observed for any of the samples.

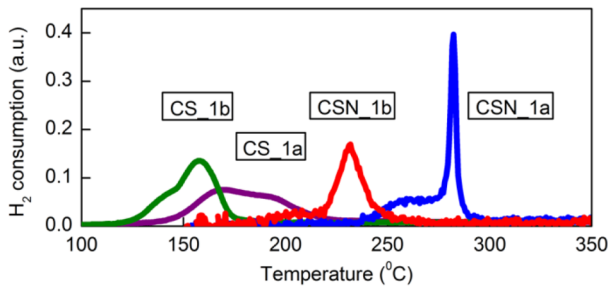

Figure 6. H_2 consumption as a function of temperature determined with TPR. For all samples, the amount of consumed hydrogen corresponds to the complete reduction of Cu^{2+} species to metallic copper.

The hydrogen consumption corresponds for all samples to the complete reduction of Cu^{2+} species to metallic copper. For CS_1a, the reduction occurred between 150 and 210 °C and for CS_1b between 130 and 170 °C. In both cases, two overlapping peaks were visible, which might be due to a stepwise reduction from CuO through monovalent Cu_2O to metallic copper. CS_1b consisted of 4−8 nm and CS_1a of 2−3 nm copper oxide particles on unfunctionalized Stöber silica. Smaller CuO particles thus required a higher temperature during reduction, consistent with literature for other metal oxides.[31] For both functionalized samples, the temperature required to reduce the copper species was higher (i.e., 230 °C and 260−280 °C), even though the particle size distribution was similar for CSN_1b compared to CS_1a. The retarded reduction for these samples is therefore not only ascribed to small copper oxide particles but also to a stabilization of copper oxide by aminopropyl groups.

TEM images of copper particles on nonfunctionalized and amine-functionalized Stöber silica after reduction are shown in Figure 7A,B. The samples were rereduced in the electron

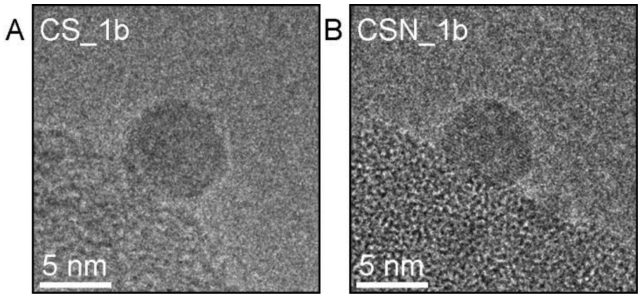

Figure 7. (A) In situ TEM image of CS_1b and (B) CSN_1b at 1 mbar of H_2 at 300 °C. For clarity, images of relatively large copper particles (∼5 nm) are shown in this figure. No dependence of the contact angle upon the particle size (2−5 nm) was found. The contact angle between the metallic copper and the support is similar for both supports (Table S1).

microscope at 1 mbar H_2 at 300 °C for half an hour to ensure that the particles were fully metallic, as evidenced by the lattice fringe spacing of 0.208 nm corresponding to the distance of the (111) planes in metallic copper (Figure 7B). Based on the densities of copper oxide and metallic copper, the change in particle size upon reduction is less than 15%. The copper oxide particle size distributions after calcination were therefore assumed to be similar to the size distribution of the copper particles after reduction. The contact angle between the metallic copper particles and the support was similar for both samples (i.e., 135° ± 20° vs 125° ± 20°, respectively; see Supporting Information). According to the Young−Duprez relation, the contact angle is determined by the surface energies of the metal and the support, and the adhesion energy between the two. A lower contact angle after functionalization therefore indicates either a lower support surface energy or a stronger adhesion energy between copper and functionalized silica. The chemical potential of a copper particle is related to the curvature of the copper surface and hence to the contact angle. Because the observed difference in contact angle is minor, the change in copper surface curvature for a given particle volume upon functionalization is also minor (see Supporting Information). Amine functionalization has thus a limited effect, if any, on the thermodynamic potential of the copper particles.

Catalytic Performance. To study the effect of the support functionalization on the stability of the copper particles during methanol synthesis, the two catalysts with similar characteristics

DOI: 10.1021/acscatal.5b00833
ACS Catal. 2015, 5, 4439−4448

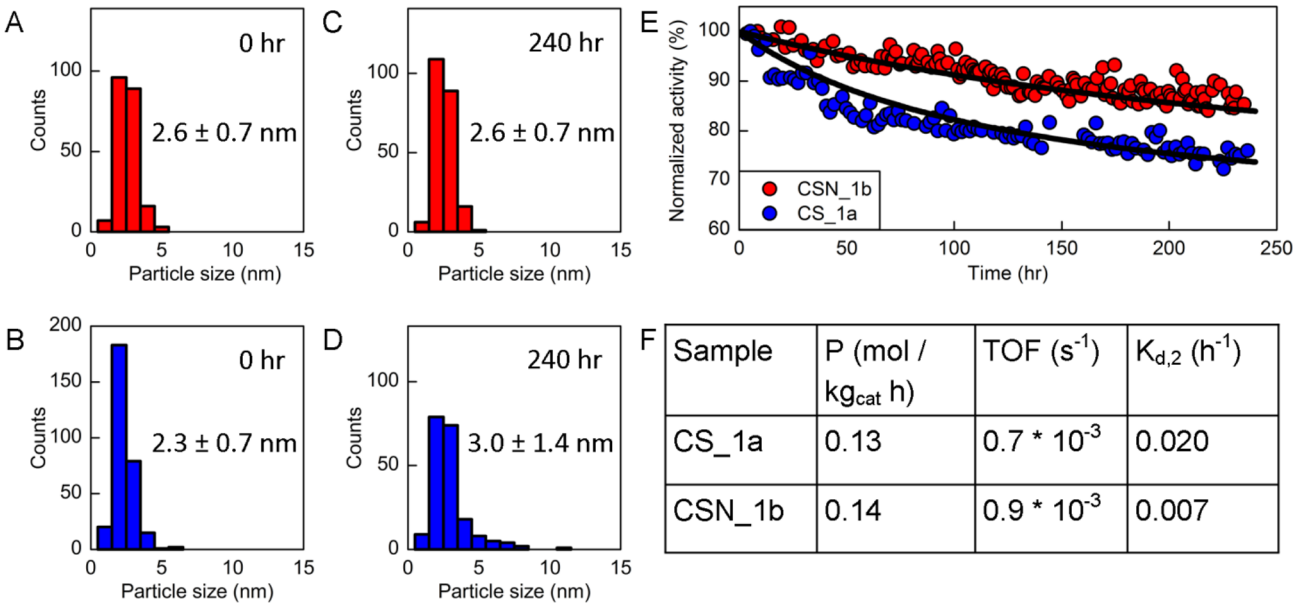

F

Sample	P (mol / kg_{cat} h)	TOF (s^{-1})	$K_{d,2}$ (h^{-1})
CS_1a	0.13	$0.7 * 10^{-3}$	0.020
CSN_1b	0.14	$0.9 * 10^{-3}$	0.007

Figure 8. (A, B) Copper oxide particle size distributions of CSN_1b (A) and CS_1a (B) before reaction. (C, D) Copper (oxide) particle size distributions of CNS_1b (C) and CS_1a (D) after reaction. (E) Normalized methanol synthesis activity over time for CSN_1b (red) and CS_1a (blue). Second-order deactivation curves were fitted for both samples (black). (F) The initial productivity (P), initial turnover frequency (TOF), and deactivation constant ($K_{d,2}$) for CSN_1b and CS_1a. Deactivation due to particle growth was faster in the case of CS_1a.

were selected: CS_1a and CSN_1b (Figure 8A–F). The initial size of the copper particles (2–3 nm, Figure 8A,B), the copper loading and the particle distribution were similar for these two catalysts. The performance of these catalysts was tested in the methanol synthesis reaction (260 °C, 40 bar, 23% CO/7% CO_2/60% H_2/10% Ar, 5% CO conversion). The selectivity toward methanol was above 95% with dimethyl ether as the main side product. The methanol synthesis productivity was therefore calculated by the CO + CO_2 conversion (Figure 8F). In literature, it has been reported that for Cu/SiO_2 catalysts, the rate of methanol formation from a mixture of CO and CO_2 is proportional to the exposed metallic copper surface area.[32] Turnover frequencies were therefore calculated with the assumption that each copper surface atom was an active site. The number of copper surface atoms was based on the TEM particle size distributions assuming fully accessible spherical particles. The TOF was similar for both catalysts, indicating that the functionalization did not change the activity of copper, and was slightly lower compared to values reported in literature for Cu/SiO_2 methanol synthesis catalysts, possibly due to the small size of the copper particles.[16b,29,32a] The TOFs were about 1 order of magnitude lower compared to an industrial-type Cu/ZnO/Al_2O_3 reference catalyst tested at the same conditions (TOF of 8.0×10^{-3} s^{-1}, see Supporting Information). This difference in activity is generally attributed to the promoting effect of ZnO.[14,16] The loss in activity with increasing time on stream was 3 times faster for the nonfunctionalized catalyst. This difference in deactivation is in line with the increase in particle size during reaction (Figure 8A–D). For CSN_1b, the particle growth was limited, whereas for CS_1a, a significant amount of larger (>3 nm) copper particles was detected after reaction. Copper particle growth was clearly more extensive for copper on silica than for copper on amine-functionalized silica.

The stability of the aminopropyl groups during copper deposition and methanol synthesis reaction was assessed with ICP (Table 3) and DRIFTS (Figure 9). The carbon and nitrogen content in the sample decreased upon copper deposition, most likely due to the relatively high calcination temperature (350 °C), resulting in the partial decomposition of aminopropyl groups. After methanol synthesis reaction for 10 days, the carbon and nitrogen content had not changed, indicating that the aminopropyl groups were stable under these conditions.

Table 3. Elemental Analysis

element	SN	CSN_1b	CSN_1b_ rxn
C (wt %)	1.36	0.84	0.89
N (wt %)	0.36	0.17	0.24

Carbon and nitrogen content of SN, CSN_1b, and CSN_1b after reaction (CSN_1b_rxn) determined with ICP.

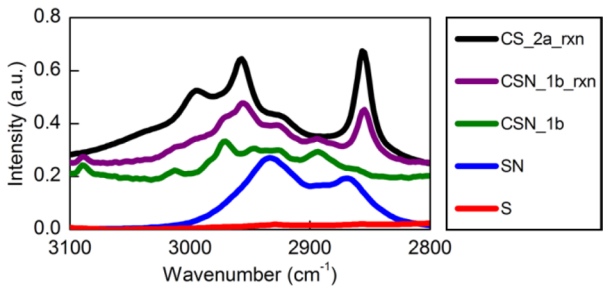

Figure 9. DRIFTS spectra between 3100 cm^{-1} and 2800 cm^{-1} of several samples at different catalyst life stages. The peaks correspond to C–H vibrations.[27] For clarity, the *y*-axis of the samples with copper has been shifted 0.25 upward. C–H vibrations of methoxy groups (2966 and 2855 cm^{-1}) were detected after methanol synthesis reaction for both copper on silica (CS_2a_rxn) and copper on amine-functionalized silica (CSN_1b_rxn).

DRIFTS spectra were recorded to verify whether N–H or C–H vibrations of the aminopropyl groups were still present after calcination and after reaction. The intensity of the N–H vibrations was already very low for SN (Figure 2B), and after calcination or reaction these peaks could no longer be detected. The main difference between the spectra of the samples at

DOI: 10.1021/acscatal.5b00833
ACS Catal. 2015, 5, 4439–4448

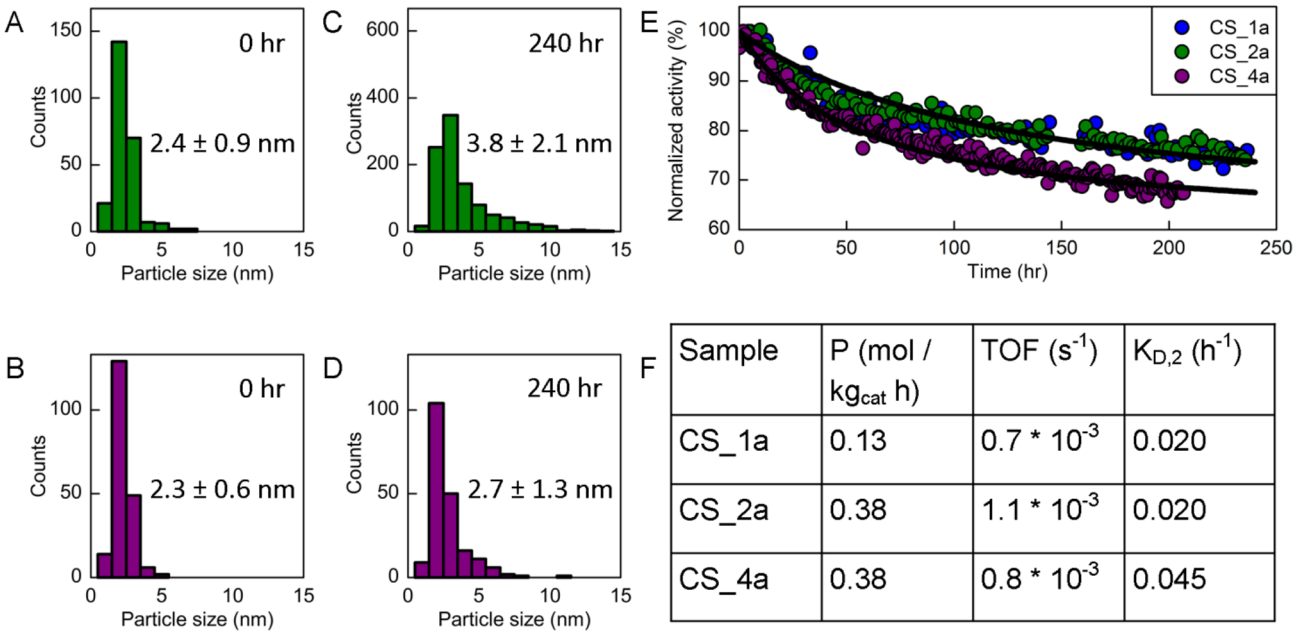

F

Sample	P (mol / kg_{cat} h)	TOF (s^{-1})	$K_{D,2}$ (h^{-1})
CS_1a	0.13	$0.7 * 10^{-3}$	0.020
CS_2a	0.38	$1.1 * 10^{-3}$	0.020
CS_4a	0.38	$0.8 * 10^{-3}$	0.045

Figure 10. (A, B) Copper oxide particle size distributions of CS_2a (A) and CS_4a (B) before reaction. (C, D) Copper (oxide) particle size distributions of CS_2a (C) and CS_4a (D) after reaction. For CS_4a, a small number of very large (>100 nm) particles were detected before and after reaction. For clarity, these particles are not included in the particle size distributions shown in B and D. Particle size distributions of CS_1a are shown in Figure 8B and D. (E) Normalized methanol synthesis activity over time for CS_1a, CS_2a and CS_4a. Second order deactivation curves were fitted for the three samples. (F) The initial productivity (P), initial turnover frequency (TOF) and deactivation constant ($K_{d,2}$) for CS_1a, CS_2a, and CS_3a.

different stages was found in the region of C−H vibrations (Figure 9). C−H vibrations were absent for the Stöber silica support (S) and appeared after functionalization (SN). After copper deposition (CSN_1b), the intensity in the C−H region decreased, in line with the loss of carbon determined with ICP, and the peak positions were changed. The peak at 2860 cm^{-1} decreased, and a new peak at 2978 cm^{-1} appeared. After reaction (CSN_1b_rxn), two additional peaks were detected: one at 2966 cm^{-1} and one at 2855 cm^{-1}. These peaks were also detected after methanol synthesis reaction of an unfunctionalized copper on silica sample (CS_2a_rxn). These peaks do not correspond to the carbon chain of the aminopropyl groups. According to literature, alkoxylation of the silica surface is possible.[33] Methanol produced during reaction can open siloxane bridges, creating methoxy and hydroxyl groups. The peaks at 2966 and 2855 cm^{-1} after methanol synthesis reaction are therefore ascribed to these methoxy groups. The intensity of the peaks at 2966 and 2855 cm^{-1} was much lower for the amine-functionalized catalyst than for the unfunctionalized catalyst. This indicates that the presence of aminopropyl groups at the surface decreased the amount of available siloxane bridges for methoxylation. Also, the total intensity of C−H vibrations was lower for CSN_1b_rxn than for CS_2a_rxn. Because the OH-stretch region was similar for both samples, this indicates that the total amount of surface functional groups (amino-propyl, methoxy, and hydroxyl groups) was lower for the functionalized sample. The functionality of the support surface was thus markedly different during methanol synthesis reaction for copper on silica than for copper on amine-functionalized silica.

Copper Particle Growth Mechanism. To understand better why copper particle growth was suppressed upon functionalization, it was necessary to obtain more information about the mechanisms involved for copper particles on silica. The effect of changing the loading on copper growth in the methanol synthesis reaction was therefore investigated (Figure 10A−F). CS_1a and CS_2a had a similar copper particle size distribution, but the loading was twice as high for CS_2a. The main difference between the two samples was therefore the particle density. CS_4a had a similar amount (2.1 wt %) of small (2−3 nm) particles as CS_2a (Figure 10A,B), next to some large copper particles (>100 nm). The catalytic performance of the three catalysts is displayed in Figure 10E,F. The turnover frequency was similar for all three catalysts. Despite the difference in particle density, the deactivation rate for CS_1a and CS_2a was also similar. Hence, the interparticle distance did not influence the rate of deactivation, although the observed increase in copper particle size was larger for CS_2a than for CS_1a (Figure 8D, 10B). The addition of very large, virtually inactive copper particles in the case of CS_4a led, however, to a faster deactivation. The particle size distributions of CS_2a and CS_4a before and after reaction are shown in Figure 10A−D. For sample CS_2a, a relatively high fraction of particles had grown larger to 4−15 nm. For sample CS_4a, just a few particles were detected with a size between 4 and 11 nm. Next to the particle size distributions shown in Figure 10B and D, some large (>100 nm) particles were also observed. The number of very large particles was insufficient to obtain a statistically relevant particle size distribution in that size range. These particles might, however, have grown larger at the expense of small 2−3 nm particles.

In the case of copper particle growth due to particle migration and coalescence, a change in interparticle spacing has been shown to lead to a faster deactivation.[11a,12a] Furthermore, the presence of a few, very large, catalytically inactive particles in the case of CS_4a is not expected to have a significant influence on the migration and coalescence of catalytically active 2−3 nm particles. It is therefore improbable that particle migration and coalescence was the dominant particle growth mechanism for these copper on silica catalysts. Ostwald ripening can, however, explain the above-mentioned results. The calculated interparticle

DOI: 10.1021/acscatal.5b00833
ACS Catal. 2015, 5, 4439−4448

distance between the 2−3 nm particles was for all samples more than two times the particle size (i.e., > 5 nm). According to the mean field approximation, there is a gradient in Ostwald ripening species just around a particle but beyond that the concentration can be considered to be independent of location.[7] Because the distances between the particles are relatively large compared to their size, they are considered to be isolated particles in a mean field of Ostwald ripening species. As a result, the deactivation did not increase upon decreasing the interparticle spacing. Also, the effect of a few, very large copper particles can be explained by Ostwald ripening, because a bimodal particle size distribution increases the thermodynamic driving force for sintering. With Ostwald ripening, the largest particles grow at the expense of the smallest particles. In the case of CS_2a, the larger 3 nm copper particles could grow at the expense of the smaller 2 nm particles to a size of 4 to 11 nm. In the case of CS_4a, very large (>100 nm) particles could grow at the expense of the small 2 and 3 nm particles, explaining the lack of 4−11 nm particles after reaction for this sample. Ostwald ripening therefore seems the most probable mechanism accounting for the present growth of the copper nanoparticles.

■ DISCUSSION

Our results show that copper on amine-functionalized silica was more resistant against deactivation than copper on unfunctionalized silica and that the growth of the copper nanoparticles in our catalysts is best explained by the Ostwald ripening mechanism. The particle size distributions and the contact angles of copper particles on the support were similar for the nonfunctionalized (CS_1a) and for the functionalized (CSN_1b) samples, meaning that the surface energy of the copper particles and hence the driving force for Ostwald ripening was similar (see Supporting Information).[7] We therefore conclude that the introduced aminopropyl groups suppressed the Ostwald ripening of copper by affecting the stability or mobility of the Ostwald ripening species.

The species that are held responsible for the Ostwald ripening are copper adsorbate species, such as CuCO.[18] Due to the relatively low reaction temperature, volatilization of copper species into the gas phase (eventually leading to a loss of copper after reaction) is unlikely. Diffusion of copper species from one particle to another therefore most likely occurred across the support surface. The increase in copper dispersion after catalyst synthesis indicated that $Cu(NO_3)_2$ and $Cu(NO_3)_2{\cdot}3H_2O$ either bind stronger to or diffuse slower on the amine-functionalized support. A strong bonding between copper species and an amine-functionalized silica is furthermore evidenced by the retarded reduction of copper oxide to metallic copper and is consistent with the finding that aminopropyl groups bind strongly to Cu^{2+} ions.[30b] Copper adsorbate species are therefore expected to bind stronger to an amine-functionalized support, increasing the activation barrier for the displacement across the support surface correspondingly.

DRIFTS showed that an amine-functionalized silica surface is rather complex with aminopropyl, hydroxyl, and methoxy groups present during reaction. Due to the high occurrence of methoxy and hydroxyl groups, it seems unlikely that the metal species can diffuse via the aminopropyl groups only. Because the copper adsorbate species are expected to bind strongly to an aminopropyl group, diffusion to another group is energetically less favorable. Second, due to the reaction of one APTES with multiple hydroxyl groups, the density of functional groups on the surface was lower for the functionalized sample (Figure 11). The distance between two neighboring functional groups became larger, lowering the chance of migration from one group to another. Due to the increased bonding between the copper adsorbate species and aminopropyl groups and due to the increased distance between different surface functional groups, the transport of Ostwald ripening species is expected to be suppressed on an amine-functionalized sample.

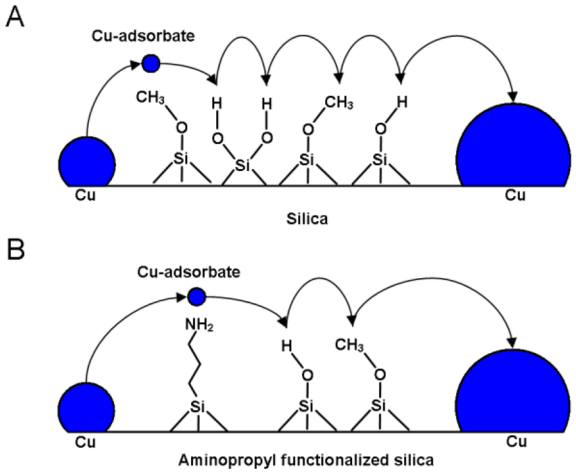

Figure 11. Schematic representation of Cu-adsorbate diffusion on silica (A) and on amine-functionalized silica (B). The effective distance between aminopropyl groups and neighboring groups is larger than between methoxy and/or hydroxyl groups. The increased distance, together with a stronger interaction between copper adsorbate species and aminopropyl groups, is expected to lead to slower diffusion of Cu-adsorbate species.

■ CONCLUSION

Copper on silica and copper on aminopropyl-functionalized silica were synthesized using impregnation of copper nitrate followed by drying, calcination, and reduction. Aminopropyl functionalization increased the dispersion of the copper due to a stronger interaction of the copper precursor with the support. Furthermore, aminopropyl functionalization retarded the reduction of the copper oxide to metallic copper, indicating a stronger interaction between copper oxide and the support. Similar particle size distributions were obtained for unfunctionalized silica and aminopropyl-functionalized silica when the N_2 flow during calcination of the former was changed to a 2% NO/N_2 flow for the latter catalyst. The support functionalization with aminopropyl groups resulted in an increased stability during methanol synthesis due to less copper particle growth. Changing the interparticle distance did not have an influence on the deactivation rate while the addition of few large particles did, indicating that Ostwald ripening is the most probable dominant particle growth mechanism for these samples. In situ TEM images showed that the contact angle between the copper particles and the support was similar for both samples. With similar size and shape, the driving force for Ostwald ripening of the copper nanoparticles was thus unchanged upon functionalization. Because the functionalization molecule, aminopropyltriethoxysilane, can react with three hydroxyl groups, the density of surface functional groups decreased upon functionalization, as was also evidenced by DRIFTS. Due to the larger distance between neighboring functional groups and due to the strong bonding of copper species with aminopropyl groups, the transport of Ostwald ripening species from one group to another is expected to be suppressed. In conclusion, these results point to

DOI: 10.1021/acscatal.5b00833
ACS Catal. 2015, 5, 4439−4448

Ostwald ripening in methanol synthesis catalysts being thus retarded by functionalization of the silica support with aminopropyl groups.

■ ASSOCIATED CONTENT

Supporting Information

The Supporting Information is available free of charge on the ACS Publications website at DOI: 10.1021/acscatal.5b00833.

Catalytic testing of aminopropyl functionalization after copper deposition, the influence of the contact angle on Ostwald ripening, contact angle measurements, electron tomography of copper on Stöber silica, calculation of catalyst activities, and synthesis of $Cu/ZnO/Al_2O_3$ (PDF)

■ AUTHOR INFORMATION

Corresponding Author

*E-mail: k.p.dejong@uu.nl.

Notes

The authors declare no competing financial interest.

■ ACKNOWLEDGMENTS

The project was supported financially by Haldor Topsoe A/S. The authors also acknowledge Haldor Topsoe A/S for access to its in situ TEM facility.

■ REFERENCES

(1) Bartholomew, C. H. *Appl. Catal., A* **1993**, *107*, 1−57.

(2) van de Loosdrecht, J.; Botes, F. G.; Ciobica, I. M.; Ferreira, A.; Gibson, P.; Moodley, D. J.; Saib, A. M.; Visagie, J. L.; Weststrate, C. J.; Niemantsverdriet, J. W. Fischer−Tropsch Synthesis: Catalysts and Chemistry. In *Comprehensive Inorganic Chemistry II*, Reedijk, J.; Poeppelmeier, K., Eds. Elsevier: Oxford, 2013; Vol. 7, pp 525−557.

(3) (a) Moulijn, J. A.; Diepen, A. E. V.; Kapteijn, F. *Appl. Catal., A* **2001**, *212*, 3−16. (b) Simonsen, S. B.; Chorkendorff, I.; Dahl, S.; Skoglundh, M.; Sehested, J.; Helveg, S. *J. Am. Chem. Soc.* **2010**, *132*, 7968−7975.

(4) Munnik, P.; Velthoen, M. E. Z.; de Jongh, P. E.; de Jong, K. P.; Gommes, C. J. *Angew. Chem.* **2014**, *126*, 9647−9651.

(5) Twigg, M. V.; Spencer, M. S. *Appl. Catal., A* **2001**, *212*, 161−174.

(6) van Santen, R. A. *Acc. Chem. Res.* **2009**, *42*, 57−66.

(7) Wynblatt, P.; Gjostein, N. A. *Prog. Solid State Chem.* **1976**, *9*, 21−58.

(8) (a) Ruckenstein, E.; Pulvermacher, B. *J. Catal.* **1973**, *29*, 224−245. (b) Harris, P. J. F. *Int. Mater. Rev.* **1995**, *40*, 97−115. (c) Munnik, P.; de Jongh, P. E.; de Jong, K. P. *J. Am. Chem. Soc.* **2014**, *136*, 7333−7340.

(9) Lifshitz, I. M.; Slyozov, V. V. *J. Phys. Chem. Solids* **1961**, *19*, 35−50.

(10) (a) Campbell, C. T.; Parker, S. C.; Starr, D. E. *Science* **2002**, *298*, 811−814. (b) Datye, A. K.; Xu, Q.; Kharas, K. C.; McCarty, J. M. *Catal. Today* **2006**, *111*, 59−67.

(11) (a) Prieto, G.; Zečević, J.; Friedrich, H.; de Jong, K. P.; de Jongh, P. E. *Nat. Mater.* **2013**, *12*, 34−39. (b) Simonsen, S. B.; Chorkendorff, I.; Dahl, S.; Skoglundh, M.; Sehested, J.; Helveg, S. *J. Catal.* **2011**, *281*, 147−155. (c) Morgenstern, K.; Rosenfeld, G.; Comsa, G. *Surf. Sci.* **1999**, *441*, 289−300.

(12) (a) Prieto, G.; Shakeri, M.; de Jong, K. P.; de Jongh, P. E. *ACS Nano* **2014**, *8*, 2522−2531. (b) Cao, A.; Lu, R.; Veser, G. *Phys. Chem. Chem. Phys.* **2010**, *12*, 13499−13510.

(13) (a) Ouyang, R.; Liu, J.-X.; Li, W.-X. *J. Am. Chem. Soc.* **2013**, *135*, 1760−1771. (b) Wallace, W. T.; Min, B. K.; Goodman, D. W. *J. Mol. Catal. A: Chem.* **2005**, *228*, 3−10.

(14) Hansen, J. B.; Hojlund Nielsen, P. E. Methanol Synthesis. In *Handbook of Heterogeneous Catalysis*, Ertl, G.; Knozinger, H.; Schuth, F.; Weltkamp, J., Eds.; Wiley-VCH: Berlin, 2008; pp 2920−2949.

(15) Olah, G. A. *Angew. Chem., Int. Ed.* **2005**, *44*, 2636−2639.

(16) (a) Behrens, M.; Studt, F.; Kasatkin, I.; Kühl, S.; Hävecker, M.; Abild-Pedersen, F.; Zander, S.; Girgsdies, F.; Kurr, P.; Kniep, B.-L.; Tovar, M.; Fischer, R. W.; Nørskov, J. K.; Schlögl, R. *Science* **2012**, *336*, 893−897. (b) Nakamura, J.; Choi, Y.; Fujitani, T. *Top. Catal.* **2003**, *22*, 277−285.

(17) (a) Wu, J.; Saito, M.; Takeuchi, M.; Watanabe, T. *Appl. Catal., A* **2001**, *218*, 235−240. (b) Kuechen, C.; Hoffmann, U. *Chem. Eng. Sci.* **1993**, *48*, 3767−3776. (c) Sun, J. T.; Metcalfe, I. S.; Sahibzada, M. *Ind. Eng. Chem. Res.* **1999**, *38*, 3868−3872.

(18) Rasmussen, D. B.; Janssens, T. V. W.; Temel, B.; Bligaard, T.; Hinnemann, B.; Helveg, S.; Sehested, J. *J. Catal.* **2012**, *293*, 205−214.

(19) (a) Campbell, C. T. *Acc. Chem. Res.* **2013**, *46*, 1712−9. (b) Campbell, C. T.; Sellers, J. R. V. *Faraday Discuss.* **2013**, *162*, 9.

(20) (a) Brühwiler, D. *Nanoscale* **2010**, *2*, 887−892. (b) Hoffmann, F.; Cornelius, M.; Morell, J.; Fröba, M. *Angew. Chem., Int. Ed.* **2006**, *45*, 3216−3251. (c) Linares, N.; Serrano, E.; Rico, M.; Mariana Balu, A.; Losada, E.; Luque, R.; García-Martínez, J. *Chem. Commun.* **2011**, *47*, 9024−9035. (d) Oliveira, R. L.; Kiyohara, P. K.; Rossi, L. M. *Green Chem.* **2010**, *12*, 144−149. (e) Jacinto, M. J.; Kiyohara, P. K.; Masunaga, S. H.; Jardim, R. F.; Rossi, L. M. *Appl. Catal., A* **2008**, *338*, 52−57.

(21) (a) Green, D. L.; Lin, J. S.; Lam, Y.-F.; Hu, M. Z.-C.; Schaefer, D. W.; Harris, M. T. *J. Colloid Interface Sci.* **2003**, *266*, 346−358. (b) Stober, W.; Fink, A.; Bohn, E. *J. Colloid Interface Sci.* **1968**, *26*, 62−69.

(22) Munnik, P.; Wolters, M.; Gabrielsson, a.; Pollington, S. D.; Headdock, G.; Bitter, J. H.; de Jongh, P. E.; de Jong, K. P. *J. Phys. Chem. C* **2011**, *115*, 14698−14706.

(23) Zhuravlev, L. T. *Colloids Surf., A* **2000**, *173*, 1−38.

(24) Eijkhoudt, R.; Smit, C. J.; Van Dillen, A. J.; Geus, J. W. *Prepr. Pap. - Am. Chem. Soc., Div Fuel Chem.* **1999**, *44*, 119−123.

(25) Brunauer, S.; Emmett, P. H.; Teller, E. *J. Am. Chem. Soc.* **1938**, *60*, 309−319.

(26) Pires, J.; Pinto, M.; Estella, J.; Echeverría, J. C. *J. Colloid Interface Sci.* **2008**, *317*, 206−213.

(27) Panchenko, V. N.; Pozimenko, V. A.; Paukshtis, E. A.; Zakharov, V. A. *Russ. J. Inorg. Chem.* **2009**, *54*, 1798−1803.

(28) Kovalchuk, T.; Sfihi, H.; Kostenko, L.; Zaitsev, V.; Fraissard, J. *J. Colloid Interface Sci.* **2006**, *302*, 214−229.

(29) Prieto, G.; Meeldijk, J. D.; de Jong, K. P.; de Jongh, P. E. *J. Catal.* **2013**, *303*, 31−40.

(30) (a) Aguado, J.; Arsuaga, J. M.; Arencibia, A.; Lindo, M.; Gascón, V. *J. Hazard. Mater.* **2009**, *163*, 213−221. (b) Deng, S.; Bai, R.; Chen, J. P. *Langmuir* **2003**, *19*, 5058−5064.

(31) Khodakov, A. Y.; Lynch, J.; Bazin, D.; Rebours, B.; Zanier, N.; Moisson, B.; Chaumette, P. *J. Catal.* **1997**, *168*, 16−25.

(32) (a) Robbins, J. L.; Iglesia, E.; Kelkar, C. P.; DeRites, B. *Catal. Lett.* **1991**, *10*, 1−10. (b) Burch, R.; Chappell, R. J. *Appl. Catal.* **1988**, *45*, 131−150.

(33) (a) Natal-Santiago, M. A.; Dumesic, J. A. *J. Catal.* **1998**, *175*, 252−268. (b) Luts, T.; Katz, A. *Top. Catal.* **2012**, *55*, 84−92. (c) Azrak, R. G.; Angell, C. L. *J. Phys. Chem.* **1973**, *77*, 3048−3052.

DOI: 10.1021/acscatal.5b00833
ACS Catal. 2015, 5, 4439−4448